Discovery of phase transitions in $Cs_6In_{0.5}W_{10.5}O_{36}$

2000 J. Phys.: Condens. Matter 12 1691

(http://iopscience.iop.org/0953-8984/12/8/312)

J. Phys.: Condens. Matter **12** (2000) 1691–1704. Printed in the UK PII: S0953-8984(00)08078-4

Discovery of phase transitions in $Cs_6In_{0.5}W_{10.5}O_{36}$

M Maczka†‡, S Kojima†, J Hanuza‡ and A Pietraszko‡

† Institute of Materials Science, University of Tsukuba, Tsukuba, Ibaraki 305-8573, Japan
‡ Institute for Low Temperature and Structure Research, Polish Academy of Sciences, PO Box 1410, 50-950 Wroclaw 2, Poland

Received 24 September 1999

Abstract. We report the first observation of structural phase transitions in $Cs_6In_{0.5}W_{10.5}O_{36}$ crystallizing with a structure intermediary between the hexagonal tungsten bronze and pyrochlore structure. The recorded Raman spectra indicate the onset of three phase transitions at about 256, 505 and above 800 K. The crystal structure above the highest temperature transition point seems to be trigonal and the Raman study suggests that below the transition point the unit cell volume is multiplied. This transition is observed also as a marked dielectric anomaly at 867 K. The character of this anomaly suggests that this transition may be ferroelectric and diffuse or order–disorder type. The heat capacity, dielectric and Raman studies show that the transition at 505 K is second order or nearly so. It is of displacive type and is induced by a soft mode, which is most likely due to a tilt of WO_6 octahedra. The low-temperature transition at 256 K has been observed in Raman experiment only. However, the observed changes in Raman spectra, which may indicate the onset of a phase transition at 256 K, are slight and therefore the confirmation of this transition needs further studies.

1. Introduction

Tungsten oxides, tungsten bronzes and tungsten bronze type compounds have received much attention due to their complex crystal chemistry and interesting properties [1, 2]. For instance, the most extensively studied hexagonal tungsten bronzes of the A_xWO_3 type, where A = K, Rb, Cs, are well known superconductors [3, 4] whereas the $M_{1-x}Ba_xNb_2O_6$ (M = Sr, Pb) niobates, crystallizing with a structure of tetragonal tungsten bronze, belong to the class of relaxor ferroelectrics which have found application in advanced technology [5]. Another interesting and little researched group of compounds consists of the A_xWO_3 type hexagonal tungsten bronzes with tungsten atoms substituted partially by atoms of lower valency. It has been shown that this partial substitution modifies significantly the physical properties of hexagonal bronzes [2, 6–10]. In contrast with the A_xWO_3 bronzes, which are nonstoichiometric compounds with metallic type conductivity, the $A_xB_yW_{1-y}O_3$ compounds (where A = alkali metal and B = Nb, Ta, Zr, In, Sc, Sn etc) are valence-balanced dielectrics. It has been also shown that these valence-balanced hexagonal bronzes undergo a number of phase transitions and may display ferroelectric or antiferroelectric properties [2, 6–9]. However, the single crystals of these compounds have been successfully grown for $K_{0.33}Nb_{0.33}W_{0.67}O_3$ and $Rb_{0.33}Nb_{0.33}W_{0.67}O_3$ only and still very little is known about properties of other valence-balanced bronzes.

In the present paper we are going to report the results of our investigation of single crystals grown in the Cs_2O–In_2O_3–WO_3 chemical system. The detailed x-ray study has revealed that the obtained crystals have $Cs_{0.5}In_{0.042}W_{0.875}O_3$ composition, instead of $Cs_{0.33}In_{0.11}W_{0.89}O_3$ expected for the hexagonal bronze structure. The crystal structure of $Cs_{0.5}In_{0.042}W_{0.875}O_3$ is

0953-8984/00/081691+14$30.00

similar to that of $Cs_6W_{11}O_{36}$ and therefore throughout the text the composition of obtained crystals will be denoted as $Cs_6In_{0.5}W_{10.5}O_{36}$. The crystal structure of $Cs_6W_{11}O_{36}$ has been studied previously [11–13], and it has been shown that this compound, together with $Cs_{8.5}W_{15}O_{48}$ and CsW_2O_6, form part of a homologous series of compounds intermediary between the hexagonal tungsten bronze and pyrochlore structure types [14]. We would like to emphasize that the present paper is the first report on Raman, heat capacity and dielectric studies performed for any member of this family of intermediary compounds. These studies indicate that although the crystal structure of $Cs_6In_{0.5}W_{10.5}O_{36}$ differs significantly from the structure of a hexagonal tungsten bronze, the physical properties of both types of tungsten compound seem to be similar to some extent. In particular, both hexagonal bronzes and $Cs_6In_{0.5}W_{10.5}O_{36}$ undergo a number of high-temperature phase transitions, which seem to be connected with tilts of WO_6 octahedra.

2. Experiment

$Cs_6In_{0.5}W_{10.5}O_{36}$ crystals were obtained by heating a mixture of $5Cs_2O + In_2O_3 + 12WO_3$ at 1000 °C for 20 h and then cooling it at a rate of 2 °C per hour. The obtained colourless crystals in the form of hexagonal prisms were separated from $Cs_2W_2O_7$ solvent by washing with hot water.

The crystal structure was determined by single-crystal x-ray diffraction with Mo Kα 0.710 73 Å radiation using the four-circle x-ray diffractometer KM4-CCD (KUMA Diffraction Company). The CCD detector of 92 mm aperture diameter was used to collect the data. The distance between the sample and detector was 70.25 mm. The data were collected in four runs at 120° ω angle using a step $\Delta\omega = 0.5°$ and 30 s exposures for one image. The structure was solved with the use of the SHELX93 (PC version) program [15], and the positions of W and Cs atoms were determined from the Patterson method. The oxygen atoms were found from difference Fourier maps.

The heat capacity measurements were performed using a Thermal Analyst 2000 calorimeter (TA Instruments). The measurements were performed on a 15.7 mg sample at heating and cooling rates of 5 K per minute. The modulation amplitude was 0.6 K every 50 seconds.

Raman spectra were obtained with a triple-grating spectrometer of additive dispersion (Jobin Yvon, T64000) with a spectral resolution of 2 cm^{-1}. The excitation source was the 514.5 nm line of an argon laser.

The dielectric constant was measured from a platelike crystal in the frequency range 1 to 800 KHz and in the temperature range 300–1000 K using HIOKI 3530 LCR HiTester. Silver electrodes were painted onto the {0001} faces (in the setting corresponding to the hexagonal structure).

3. Results and discussion

3.1. Structural analysis

The crystal structure of $Cs_6In_{0.5}W_{10.5}O_{36}$ may be determined either as monoclinic, $C2/m$ with lattice parameters $a = 12.631$, $b = 7.295$, $c = 18.989$ Å and $\beta = 102.77°$ ($Z = 2$), or as trigonal, $R\bar{3}$ with lattice parameters $a = 7.294$, $b = 7.294$, $c = 55.556$ Å ($Z = 3$). The final discrepancy factors for monoclinic symmetry was $R = 0.059$ and for trigonal symmetry $R = 0.055$. The similar problem of choosing the right crystal symmetry occurred also for $Cs_6W_{11}O_{36}$. The first work reporting the crystal structure of $Cs_6W_{11}O_{36}$ suggested that it was

Table 1. Crystal data and structure refinement parameters for $Cs_6In_{0.5}W_{10.5}O_{36}$.

Empirical formula	$Cs_6In_{0.5}W_{10.5}O_{36}$
Formula weight	3361.30
Temperature	293(2) K
Wavelength	0.710 73 Å
Crystal system, space group	Trigonal, $R\bar{3}$
Unit cell dimensions	$a = 7.2940(10)$ Å $\alpha = 90^\circ$
	$b = 7.2940(10)$ Å $\beta = 90^\circ$
	$c = 55.556(11)$ Å $\gamma = 120^\circ$
Volume	2559.7(7) Å^3
Z, calculated density	3, 6.542 Mg m^{-3}
Absorption coefficient	41.977 mm^{-1}
$F(000)$	4259
Crystal size	$0.25 \times 0.32 \times 0.05$ mm^3
θ range for data collection	4.89 to 23.26°
Index ranges	$-8 \leqslant h \leqslant 8$, $-7 \leqslant k \leqslant 7$, $-61 \leqslant l \leqslant 61$
Reflections collected/unique	2797/789 (R(int) = 0.0510)
Completeness to $\theta = 23.26$	95.9%
Refinement method	Full-matrix least squares on F^2
Data/restraints/parameters	789/0/86
Goodness of fit on F^2	1.317
Final R indices ($I > 2\sigma(I)$)	$R_1 = 0.0548$, $wR_2 = 0.1291$
R indices (all data)	$R_1 = 0.0600$, $wR_2 = 0.1322$
Extinction coefficient	0.000 000(5)
Largest diff. peak and hole	4.049 and −3.517 e Å^{-3}

Table 2. Atomic coordinates ($\times 10^4$) and equivalent isotropic displacement parameters (Å$^2 \times 10^3$) for $Cs_6In_{0.5}W_{10.5}O_{36}$. U(eq) is defined as one third of the trace of the orthogonalized U_{ij} tensor.

	x	y	z	U(eq)
W(1)	3333	6667	2775(1)	7(1)
W(2)	1667	8333	3333	22(1)
W(3)	9943(1)	4972(1)	2234(1)	11(1)
In(1)	9943(1)	4972(1)	2234(1)	11(1)
Cs(1)	6667	3333	2914(1)	21(1)
Cs(2)	0	0	1860(1)	26(1)
Cs(3)	0	10 000	2667(1)	26(1)
Cs(4)	13 333	6667	1667	40(4)
O(1)	2118(8)	7872(8)	3016(1)	11(2)
O(2)	9346(9)	4665(8)	1929(1)	17(2)
O(3)	4567(9)	5413(9)	2607(1)	14(2)
O(4)	2100(8)	4208(8)	2219(1)	8(2)
O(5)	7889(8)	2122(8)	2330(1)	11(2)
O(6)	864(8)	5429(8)	3408(1)	13(2)

best described as monoclinic [11]. However, the recent reports suggested that the structure of $Cs_6W_{11}O_{36}$ was described as monoclinic incorrectly and that the correct space group was trigonal, $R\bar{3}c$ [12, 13]. We may suppose, therefore, that also in case of $Cs_6In_{0.5}W_{10.5}O_{36}$ the crystal structure should be described as trigonal rather than monoclinic. Table 1 summarizes the determined crystal data for the $R\bar{3}$ structure and gives the structure refinement parameters. The final atomic coordinates and selected interatomic distances are presented in tables 2 and 3.

Table 3. Selected bond lengths (Å) for $Cs_6In_{0.5}W_{10.5}O_{36}$.

W(1)–O(3) No 1	1.828(7)	Cs(1)–O(3) No 7	3.143(7)
W(1)–O(3) No 2	1.828(7)	Cs(1)–O(3) No 6	3.143(7)
W(1)–O(3)	1.828(7)	Cs(1)–O(3)	3.143(7)
W(1)–O(1)	2.031(7)	Cs(1)–O(6) No 8	3.269(6)
W(1)–O(1) No 1	2.031(7)	Cs(1)–O(6) No 9	3.269(6)
W(1)–O(1) No 2	2.031(7)	Cs(1)–O(6) No 10	3.269(6)
W(2)–O(1) No 3	1.854(6)	Cs(2)–O(2) No 16	3.045(6)
W(2)–O(1)	1.854(6)	Cs(2)–O(2) No 17	3.045(6)
W(2)–O(6) No 1	1.935(7)	Cs(2)–O(2) No 18	3.045(6)
W(2)–O(6) No 4	1.935(7)	Cs(2)–O(4)	3.324(5)
W(2)–O(6)	1.940(6)	Cs(2)–O(4) No 11	3.324(5)
W(2)–O(6) No 3	1.940(6)	Cs(2)–O(4) No 19	3.324(5)
W(3)–O(2)	1.736(6)	Cs(3)–O(5) No 11	3.264(7)
W(3)–O(4) No 5	1.916(7)	Cs(3)–O(5) No 12	3.264(7)
W(3)–O(4) No 6	1.921(6)	Cs(3)–O(5) No 13	3.264(7)
W(3)–O(5)	1.932(5)	Cs(3)–O(1) No 14	3.312(7)
W(3)–O(5) No 7	1.939(5)	Cs(3)–O(1)	3.312(7)
W(3)–O(3) No 6	2.152(6)	Cs(3)–O(1) No 15	3.312(7)

Symmetry transformations used to generate equivalent atoms: No 1: $-x+y, -x+1, z$; No 2: $-y+1, x-y+1, z$; No 3: $-x+1/3, -y+5/3, -z+2/3$; No 4: $x-y+1/3, x+2/3, -z+2/3$; No 5: $x+1, y, z$; No 6: $-x+y+1, -x+1, z$; No 7: $-y+1, x-y, z$; No 8: $x-y+4/3, x+2/3, -z+2/3$; No 9: $-x+1/3, -y+2/3, -z+2/3$; No 10: $y+1/3, -x+y-1/3, -z+2/3$; No 11: $-y, x-y, z$; No 12: $x-1, y+1, z$; No 13: $-x+y+1, -x+2, z$; No 14: $-y+1, x-y+2, z$; No 15: $-x+y-1, -x+1, z$; No 16: $y-1/3, -x+y+1/3, -z+1/3$; No 17: $-x+2/3, -y+1/3, -z+1/3$; No 18: $x-y-1/3, x-2/3, -z+1/3$; No 19: $-x+y, -x, z$.

The crystal structure of $Cs_6In_{0.5}W_{10.5}O_{36}$ may be described as consisting of complex layers, which are built up of three hexagonal tungsten bronze layers connected by two intermediary layers of WO_6 octahedra (see figures 1 and 2). Caesium atoms are located both as spacers between the complex layers and within these layers. The In atoms occupy statistically the same positions as the W(3) atoms. The framework of the crystal structure is very similar to the crystal structure of $Cs_6W_{11}O_{36}$ [11, 12], with the difference that in the present case the determined space group is $R\bar{3}$ instead of $R\bar{3}c$ and the unit cell contains three formula units instead of six. We would like to point out, however, that $Cs_6In_{0.5}W_{10.5}O_{36}$ undergoes at least two high-temperature phase transitions (see discussion below) and a few facts suggest that the determined trigonal structure may apply to a high-temperature phase only. One of these facts is the presence of superstructure reflections, which were a few times smaller than the main reflections. These superstructure reflections indicate probably a pseudo-hexagonal twinning. The other indications that the ambient temperature symmetry may be lower than trigonal are provided by Raman measurements and will be discussed in the next sections of this paper.

3.2. Heat capacity measurements

The heat capacity measurements, performed in the 130–750 K range, revealed the presence of only one clear anomaly around 508 K. The relevant part of the heat capacity curve is presented in figure 3. This anomaly shows a small thermal hysteresis, i.e. it is observed at 506.4 K for cooling runs and at 510.2 K for heating runs. The shape of the measured anomaly and the observed hysteresis suggest that the studied crystal undergoes a weakly first-order phase transition at 508.3 K. The calculated enthalpy and entropy of this transition is 0.039 J g^{-1} and 7.7×10^{-5} J g^{-1} K^{-1}.

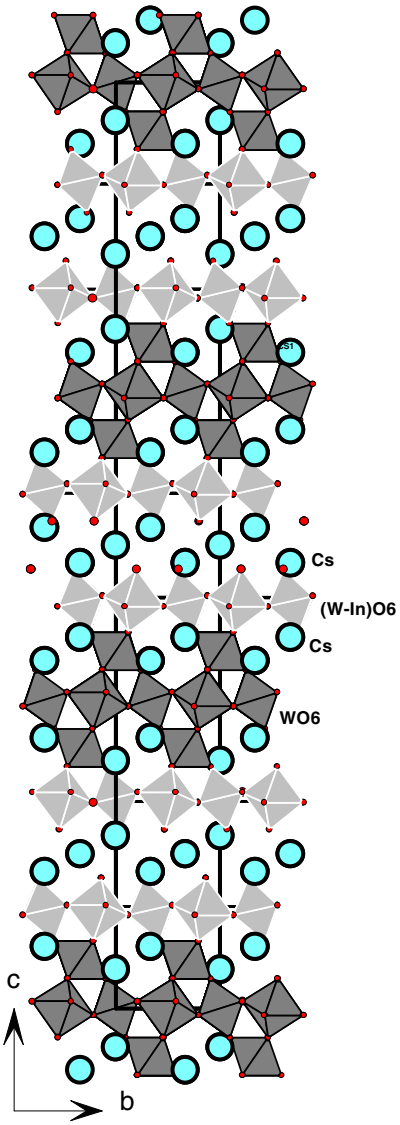

Figure 1. The crystal structure of $Cs_6In_{0.5}W_{10.5}O_{36}$ projected on the yz plane.

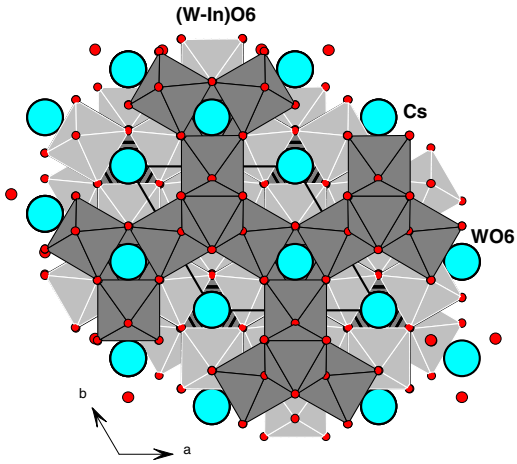

Figure 2. The crystal structure of $Cs_6In_{0.5}W_{10.5}O_{36}$ projected on the xy plane.

3.3. Dielectric measurements

The temperature dependence of the dielectric constant along the c axis reveals the presence of two marked anomalies (see figures 4 and 5). The first, weak and narrow anomaly is observed at 506 K. A second anomaly, observed at 867 K, is much stronger and very broad. Both anomalies exhibit a pronounced dielectric dispersion. The character of these anomalies suggests that they correspond to phase transitions which are second order or nearly so. The relatively high dielectric constant and the marked broadness of the dielectric peak at 867 K indicate that the phase transition at 867 K may be of the ferroelectric type, and diffuse or order–disorder

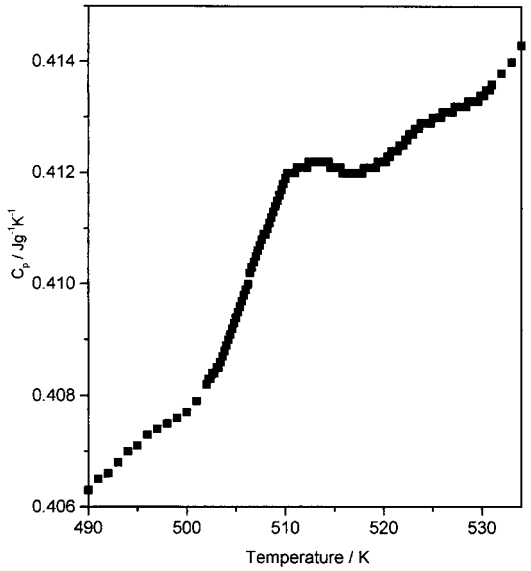

Figure 3. Measured heat capacity showing the anomaly around 508 K.

type. It is worth to mention that a very similar dielectric characteristic was observed for $K_{0.33}Nb_{0.33}W_{0.67}O_3$ and $Rb_{0.33}Nb_{0.33}W_{0.67}O_3$ crystallizing with a hexagonal tungsten bronze structure. I.e. the dielectric constant along the c axis exhibited strong dielectric anomalies around 850–1100 K and weak anomalies around 550–650 K [6, 16].

3.4. Raman spectra

The ambient-temperature spectra are presented in figure 6 and vibrational frequencies are listed in table 4. According to the factor group analysis (see table 5), 25 A_g and 25 E_g modes should be observed for the $R\bar{3}$ structure of $Cs_6In_{0.5}W_{10.5}O_{36}$ in the Raman experiment. However, the number of observed modes, about 35 at ambient temperature, is significantly smaller than expected. This may be attributed to accidental degeneracy of a number of modes. Moreover, some weak bands are most likely overlapped by much stronger bands.

The observed bands in the 580–1000 cm^{-1} region may be assigned to the stretching vibrations of the terminal W–O and bridging W–O–W bonds. Since the terminal W(3)–O(2) bonds are much shorter than the other W–O bonds (see table 3), we may assign unambiguously the two highest frequency bands at 946 and 969 cm^{-1} to the terminal W–O stretching vibrations. This assignment is supported by the results of Raman investigation of WO_3, which has no terminal bonds, and IR studies of oxidized Cs_xWO_3 and A_xMoO_3 bronzes (A = alkali atom), which have terminal bonds. In the former case, no bands were observed above 810 cm^{-1} [17], whereas sharp bands in the 900–1000 cm^{-1} region were observed for the latter compounds [18, 19]. Since the terminal W(3)–O(2) bonds are directed almost parallel to the z axis, the 946 and 969 cm^{-1} bands show most of their intensities for the $x(zz)\bar{x}$ polarization configuration. The remaining stretching bands may be assigned to the bridging W–O–W modes. The group of poorly resolved bands at 580–720 cm^{-1} is active mainly for the $z(xx)\bar{z}$ polarization whereas the 852 cm^{-1} band for the $x(zz)\bar{x}$ polarization. Such a behaviour suggests that the 580–720 cm^{-1} bands originate from the stretching vibrations of long W(3)–O(4), W(3)–O(5) and W(2)–O(6) bonds (with the W–O distance of 1.916–1.940 Å), which are directed almost perpendicular to

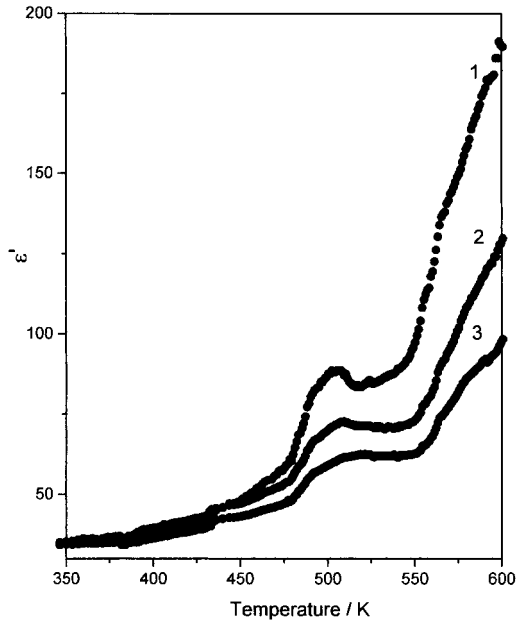

Figure 4. The dielectric constant in the 350–600 K range measured along the *c* axis with frequency of 4 (1), 10 (2) and 20 KHz (3).

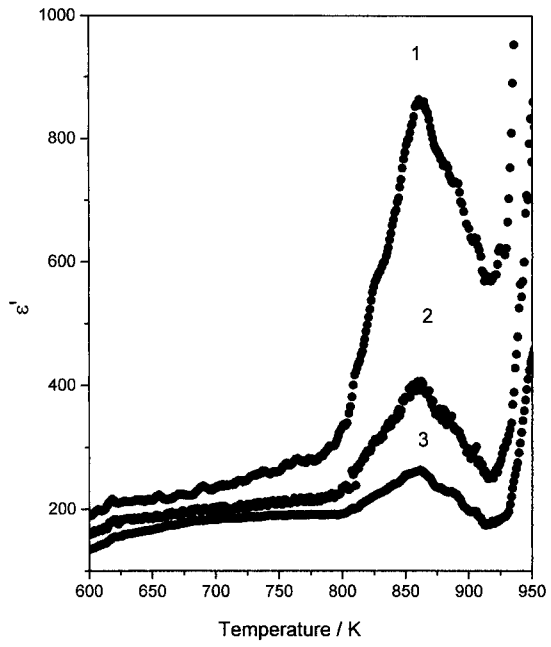

Figure 5. The dielectric constant in the 600–950 K range measured along the *c* axis with frequency of 4 (1), 10 (2) and 20 KHz (3).

the *z* axis. The single band at 852 cm^{-1} may be assigned most likely to vibrations of medium strong W(2)–O(1) and W(1)–O(3) bonds (with the W–O distance of 1.828–1.854 Å).

Table 4. Vibrational modes (in cm^{-1}) at ambient temperature and different polarization configurations.

$z(xx)\bar{z}$	$z(xy)\bar{z}$	$x(zz)\bar{x}$	$x(zy)\bar{x}$	Assignment
970m	969m	969s	968m	terminal W–O stretching mode
—	—	946w	944vw	terminal W–O stretching mode
853m	853m	852s	853m	
722s	722s	721w	720w	
701w	—	—	—	
690m	689m	693w	694w	W–O–W bridging stretching modes
669m	669m	670vw	669w	
631m	632m	626vw	630vw	
584w	586w	587vw	585vw	
483vw	—	—	—	
456vw	455vw	—	—	
444vw	—	449vw	444w	
433vw	—	433vw	—	
416vw	—	—	418w	
406vw	—	—	—	
385vw	386vw	385vw	385w	
—	—	—	365w	
348vw	—	346w	346sh	
338w	338w	337w	337w	
284vw	284vw	—	284w	W–O and W–O–W bending modes,
247w	246w	250w	250w	$L(WO_6)$ and $T'(WO_6)$
231m	230w	225m	226m	
—	—	—	220m	
205s	205s	204w	205w	
174sh	175sh	171m	171m	
168s	168s	—	—	
150vw	152vw	150vw	—	
129m	129m	129m	129m	
92s	92s	91w	92m	
77m	77m	77s	77m	
72sh	72sh	—	—	
—	—	58s	58m	
—	—	51s	51m	$T'(Cs^+)$
—	—	45sh	46m	
—	—	31w	31w	
46vs	46vs	—	—	soft mode

The modes below 500 cm^{-1} describe the bending vibrations of the terminal W–O and bridging W–O–W bonds, librational and translational motions of WO_6 octahedra and translational motions of Cs^+ ions. The precise assignment of observed bands to the respective lattice or bending modes is meaningless since we may expect a high degree of coupling among these modes. One can notice, however, that whereas the bands above 100 cm^{-1} are broad, most of the bands below 100 cm^{-1} are very narrow. These narrow modes have probably a large contribution of translational motions of heavy and weakly bonded Cs^+ ions. It should be also mentioned that one of the low-frequency modes, observed at 46 cm^{-1} at ambient temperature, is unusually strong. The origin of this mode, active for the $z(xx)\bar{z}$ polarization only, will be discussed below. It may be also noticed that measurements performed with the

Table 5. Factor group analysis for $Cs_6In_{0.5}W_{10.5}O_{36}$.

					Activity	
S_6	n(N)	n(W)	n(O)	n(Cs)	IR	Raman
A_g	25	4	18	3	—	$xx + yy, zz$
E_g	25	4	18	3	—	$xx - yy, xy, xz, yz$
A_u	28	7	18	3	z	—
E_u	28	7	18	3	x, y	—

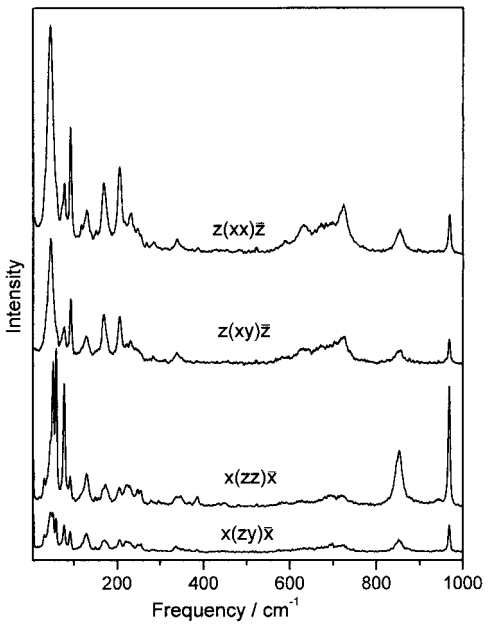

Figure 6. Ambient temperature polarized Raman spectra of $Cs_6In_{0.5}W_{10.5}O_{36}$.

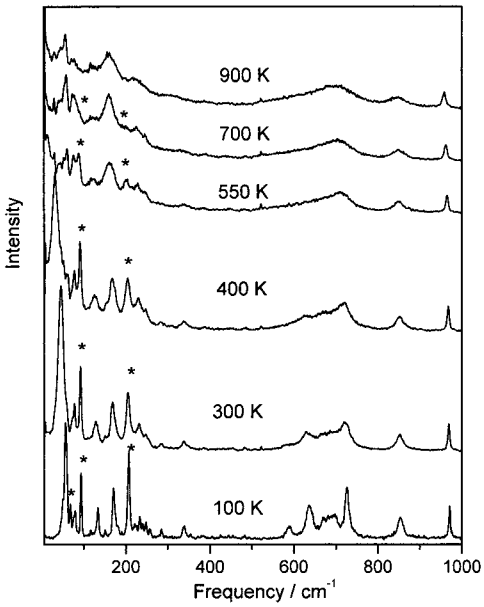

Figure 7. Temperature dependent Raman spectra for $z(xx + xy)\bar{z}$ polarization.

use of polarized light suggest that the ambient temperature structure is lower than trigonal. In case of a single trigonal crystal, for the $z(xx)\bar{z}$ polarization both A_g and E_g modes should be observed, whereas for the $z(xy)\bar{z}$ polarization A_g modes are forbidden by selection rules. Similarly, for the $x(zz)\bar{x}$ polarization only A_g and for the $x(zy)\bar{x}$ polarization only E_g modes should be observed. Our measurements show, however, that the $z(xx)\bar{z}$ and $z(xy)\bar{z}$ or $x(zz)\bar{x}$ and $x(zy)\bar{x}$ spectra are very similar to each other. Such a result favours the conclusion that the trigonal structure may apply only to a high-temperature phase of $Cs_6In_{0.5}W_{10.5}O_{36}$.

Let us now discuss the temperature dependence of the Raman spectra. The measured spectra (figure 7) show that when temperature increases from 100 to 900 K, most bands in the 300–1000 cm^{-1} region exhibit only minor frequency changes (figure 8). The number of observed modes decreases from 18 at 100 K to 7 at 900 K. The decrease in number of resolved bands is due primarily to the pronounced broadening of measured bands at higher temperatures. However, a few observed bands seem to disappear when temperature increases suggesting the presence of high-temperature phase transitions. This is the case, for example, for the W–O–W stretching modes at 588 and 637 cm^{-1} (see figure 7). Pronounced changes, which indicate that this crystal undergoes a number of successive phase transitions, are much

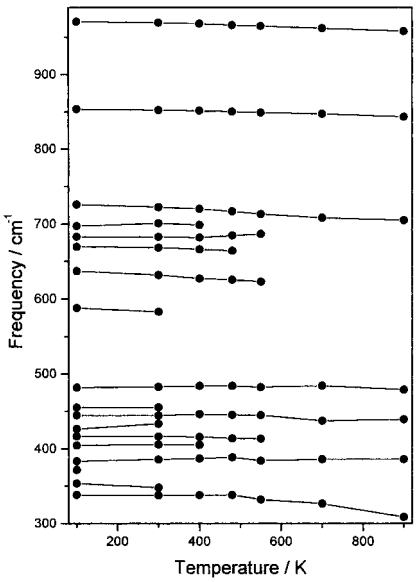

Figure 8. Temperature dependence of frequency for the 300–1000 cm^{-1} modes. Solid lines are to guide the eye.

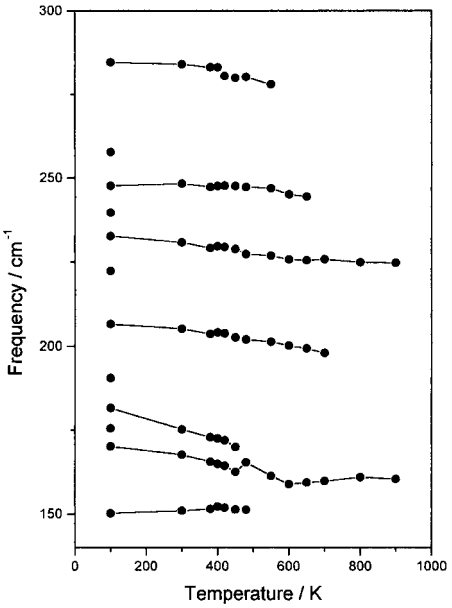

Figure 9. Temperature dependence of frequency for the 150–300 cm^{-1} modes. Solid lines are to guide the eye.

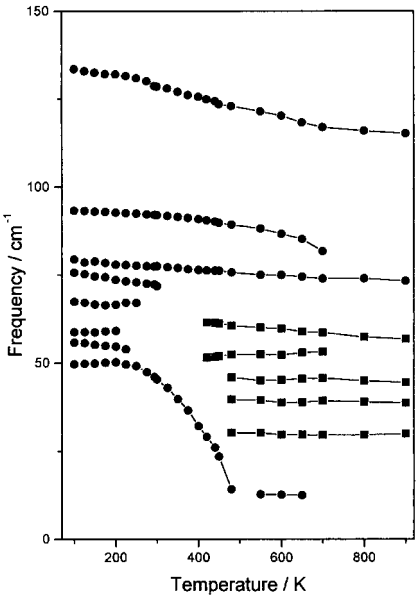

Figure 10. Temperature dependence of frequency for the 8–150 cm^{-1} modes. Solid lines are to guide the eye.

more clearly observed in the frequency region below 300 cm^{-1}. Firstly, significant softening with increasing temperature is noticed for a few modes (see figures 7–10). Especially marked temperature dependence is observed for the strong and broad mode, located at 46 cm^{-1} at ambient temperature, which shows a typical soft-mode behaviour. Secondly, a few modes, indicated in figure 7 by asterisks, show continuous intensity decrease with increasing temperature.

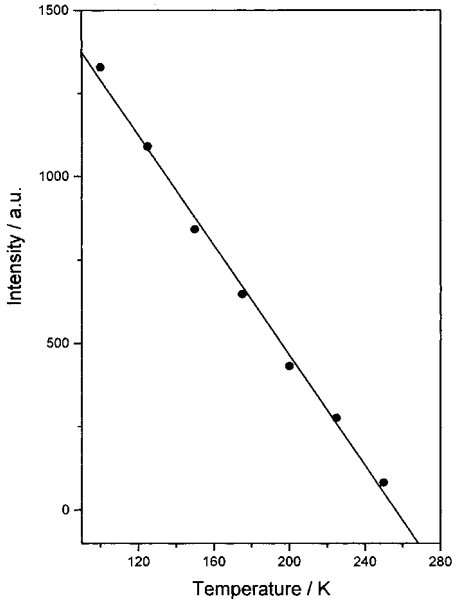

Figure 11. Integrated intensity of the 67 cm^{-1} mode as a function of temperature.

The detailed analysis of temperature dependence of the Raman spectra reveals that the first phase transition may take place around ambient temperature. This transition manifests itself by splitting of the 46 cm^{-1} mode into three components and appearance of the 67 cm^{-1} mode below the phase transition temperature (see figure 10). The plot of the integrated intensity for the 67 cm^{-1} mode (divided by $n(\omega) + 1$, where $n(\omega)$ is the Bose–Einstein factor) shows that this intensity is approximately a linear function of temperature (figure 11). A least squares fitting to the data shows that the transition temperature is 256.3 ± 5.6 K. We should point out, however, that the observed changes in the Raman spectra are relatively slight and therefore the confirmation of this transition needs further studies.

The second transition is indicated by the marked softening of the 46 cm^{-1} mode with increasing temperature (see figures 7 and 10). The temperature dependence of the soft mode shows that it is underdamped and therefore its frequency was extracted from the fitting to the Lorentzian band shape. The squared frequency of the soft mode is approximately a linear function of temperature and the fitting gives a 505.1 ± 6.6 K transition temperature (figure 12). The obtained transition temperature is in agreement with the heat capacity and dielectric studies, showing anomalies at 508.2 K and 506 K, respectively. The presence of the soft mode and lack of any jump changes indicate that this transition is displacive and second or nearly second order. The very strong intensity of the soft mode suggests that this transition is not induced by shifts of weakly polarizable Cs^+ ions, but is driven by instability of a mode involving movements of W atoms or rotations of WO_6 octahedra. The studies of WO_3 and A_xWO_3 tungsten bronzes, where A = alkali metal, Sn and In, indicate that the second possibility is more likely because phase transitions in these compounds involve usually a tilt of WO_6 octahedra [1]. It should be also noticed that although the frequency of the soft mode decreases to zero, when the 506 K transition temperature is approached from below, a weak band around 12 cm^{-1} remains up to 700 K. This band exhibits no softening in the 550–700 K range. Its intensity decreases, however, with increasing temperature and it disappears completely around 700 K.

As temperature increases further, the crystal exhibits a third phase transition. This transition manifests itself most clearly by disappearance of the 90 and 207 cm^{-1} bands, and by

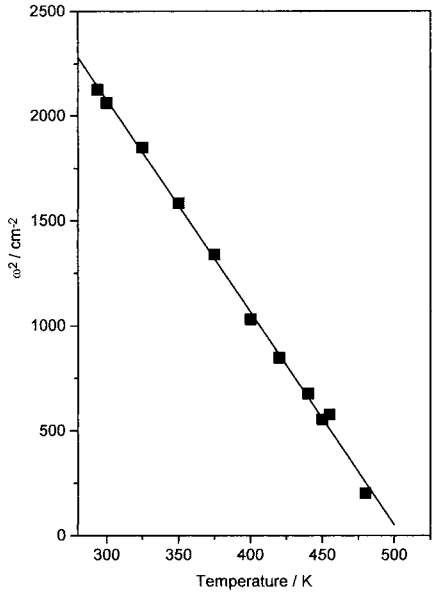

Figure 12. The squared frequency of the soft mode as a function of temperature.

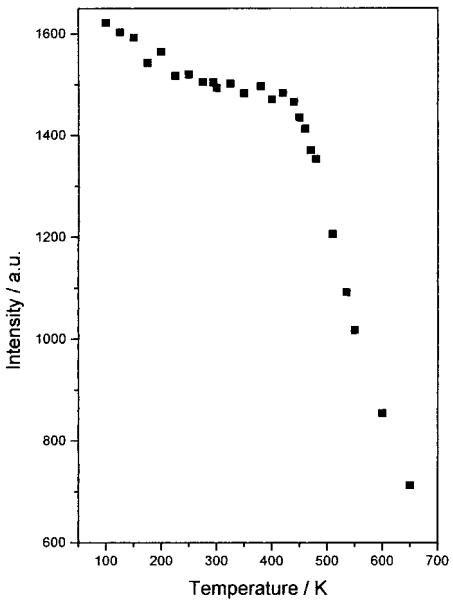

Figure 13. Integrated intensity of the 90 cm^{-1} mode as a function of temperature.

strong intensity change of the 73 cm^{-1} mode. The plot of the 90 cm^{-1} mode intensity against temperature shows that above 450 K the intensity decrease is approximately a linear function of temperature (figure 13). The extrapolation of the data shows that this band disappears completely at about 815 ± 27 K. One should remember, however, that due to very weak intensity and large bandwidth of the discussed band at high temperatures, the analysis of intensity is associated with large error. Therefore, we may suppose that the observed changes in Raman spectra have the same origin as the broad and relatively strong dielectric anomaly around 867 K.

4. Conclusion

The dielectric, heat capacity and Raman studies reveal the existence of three reversible phase transitions in $Cs_6In_{0.5}W_{10.5}O_{36}$ at 256, 506 and 867 K. All the three transitions seem to be of second order or nearly so. The appearance of new Raman-active vibrations, as a result of the 867 K transition, suggests that below the transition point the unit cell volume is multiplied. If it is really so, the ambient temperature structure must be different from the determined $R\bar{3}$ since for the $R\bar{3}$ symmetry the primitive cell contains only one formula unit. The appearance of new Raman modes is, therefore, yet another indication that the $R\bar{3}$ structure may apply to a high-temperature phase only. The dielectric measurements show that the transitions at 506 and 867 K may be antiferroelectric or ferroelectric, and that the latter transition is of diffuse or order–disorder type. The 506 K transition is of displacive type. This is indicated by the temperature behaviour of the intense low-frequency mode, observed at 46 cm^{-1} at ambient temperature, which softens markedly as temperature approaches 506 K. This transition involves probably a tilt of WO_6 octahedra.

Finally, we have shown that the $Cs_6In_{0.5}W_{10.5}O_{36}$ crystal exhibits an interesting sequence of structural phase transitions. However, the symmetries of different phases cannot be discussed since even the structure of a prototype high-temperature phase is not known. The solution of this problem needs much more studies, including high-temperature x-ray diffraction measurements. At the present moment we may only predict that the $R\bar{3}$ structure determined at ambient temperature may apply actually to the prototype high-temperature phase, since the presence of superstructure reflections and Raman study strongly suggest that the ambient-temperature structure is lower than trigonal. Such a conclusion is also supported by the results of x-ray investigations of other tungsten oxides and tungsten bronzes which showed that usually the structural arrangement was pseudo-symmetrical, i.e. atomic positions were approximately those of a basic structure of higher symmetry [1].

Acknowledgments

This work was partially supported by the Foundation for Advancement of International Science and the Polish State Committee for Scientific Research, grant No 3 TO9B 090 15. One of the authors (Miroslaw Maczka) acknowledges the Japanese Society for the Promotion of Science for the financial support of his stay at the University of Tsukuba.

References

[1] Labbe P 1992 *Key Eng. Mater.* **68** 293
[2] Isupov V A 1985 *Ferroelectrics* **65** 181
[3] Caldwell L H, Morris R C and Houlton W G 1981 *Phys. Rev.* B **23** 2219
[4] Skokan M R, Moulton W G and Morris R C 1979 *Phys. Rev.* B **20** 3670
[5] Ye Z G 1998 *Key Eng. Mater.* **155/156** 81
[6] Yanovskii V K, Voronkova V I and Stefanovich S Yu 1977 *Sov. Phys.–Crystallogr.* **22** 731
[7] Minaeva G N, Voronkova V I and Yanovskii V K 1979 *Sov. Phys.–Crystallogr.* **24** 157
[8] Stefanovich S Yu, Bazarova Zh G, Batueva I S and Mokhosoev M V 1991 *Sov. Phys.–Crystallogr.* **35** 692
[9] Klimova I P, Voronkova B I and Yanovskii V K 1995 *Neorg. Mater.* **31** 262
[10] Tao Y, Hu Mei-Shen and Feng D 1988 *Phys. Status Solidi* a **109** 435
[11] Okada K, Marumo F and Iwai S 1978 *Acta Crystallogr.* B **34** 50
[12] Marsh R E 1995 *Acta Crystallogr.* B **51** 300
[13] Solodovnikov S F, Mankova O A, Solodovnikova Z A, Ivannikova N V and Alekseev I 1996 *Zh. Struk. Khim.* **37** 756
[14] Cava R J, Roth R S, Siegrist T, Hessen B, Krajewski J J and Peck W P 1993 *J. Solid State Chem.* **103** 359

[15] Sheldrick G M *SHELX-93 and SHELX-97 Program for the Refinement of Crystal Structures*
[16] Klimova I P, Voronkova V I, Okonenko S A, Stefanovich S Yu and Yanovskii V K 1980 *Sov. Phys.–Crystallogr.* **25** 67
[17] Salje E 1975 *Acta Crystallogr.* A **31** 360
[18] Mortimer R, Powell J G, Greenblatt M, McCaroll W H and Ramanujachary K V 1993 *Chem. Soc. Faraday Trans.* **89** 3603
[19] Oi J, Kishimoto A and Kudo T 1993 *J. Solid State Chem.* **103** 176